INSTITUTE OF PHYSICS PUBLISHING JOURNAL OF PHYSICS D: APPLIED PHYSICS

J. Phys. D: Appl. Phys. **36** (2003) 1729–1738 PII: S0022-3727(03)55708-4

# Applications of cost-effective spectral imaging microscopy in cancer research

**P R Barber[1,3], B Vojnovic[1], G Atkin[1], F M Daley[1], S A Everett[1], G D Wilson[2] and J D Gilbey[1]**

[1] Gray Cancer Institute, Mount Vernon Hospital, Northwood, Middlesex HA6 2JR, UK
[2] Karmanos Cancer Institute, Wayne State University, Hudson Webber Building, 4100 John R, Detroit, MI 48201-2013, USA

E-mail: barber@gci.ac.uk

Received 6 November 2002
Published 1 July 2003
Online at stacks.iop.org/JPhysD/36/1729

**Abstract**

The application of a cost-effective spectral imager to spatially segmenting absorptive and fluorescent chemical probes on the basis of their spectral characteristics has been demonstrated. The imager comprises a computer-controlled spectrally selective element that allows random access to a bandwidth of 15 nm between 400 and 700 nm. Further, the use of linear un-mixing of the spectral response of a sample at a single pixel has been facilitated using non-negative least squares fitting. Examples are given showing the separation of dye distributions, such as immunohistochemical markers for tumour hypoxia, from multiply stained thin tissue sections, imaged by trans-illumination microscopy. A quantitative study is also presented that shows a correlation between staining intensity and normal versus tumour tissue, and the advantage of reducing the amount of data captured for a particular study is also demonstrated. An example of the application to fluorescence microscopy is also given, showing the separation of green fluorescent protein, Cy3 and Cy5 at a single pixel. The system has been validated against samples of known optical density and of known overlapping combinations of coloured filters. These results confirm the ability of this technique to separate spectral responses that cannot be resolved with conventional colour imaging.

## 1. Introduction

Spectral imaging generates a three-dimensional data set that represents the sample both spatially and spectrally. Traditional microscopy offers high spatial resolution by coupling a high-resolution imager, typically with a minimum of 500 × 500 pixels, to the output port of the microscope. The use of a colour imager provides some spectral information in the form of three broad, and partially overlapping, spectral bands covering the red, green and blue (RGB) regions. In contrast, spectral imaging can provide narrow bandwidth information at a high number of wavelengths spanning the visible spectrum. In the field of microscopy, the additional information available though this technique is not only a valuable tool for visualizing previously invisible structures but is also of great advantage when the goals are automation and quantitative measurement. This paper describes some applications of a spectral imaging device to histology and to fluorescence microscopy. The applications involve the use of a multiplicity of markers where co-localization and segmentation of the markers is of interest.

In histology the aim is to segment and separate differently coloured dyes that stain thin ($<30\,\mu$m) sections of biological tissue. These histo-chemical markers can reveal specific cellular and tissue characteristics and are commonly used as a critical form of patient diagnosis. A spectral imaging microscope is capable of resolving spectral changes in optical density (OD) and can therefore be useful in segmenting these dyes, especially when their apparent colours are similar. Most dyes used in histology have very broad absorption spectra and it is this feature that limits the applicability of conventional RGB camera. In general these dyes have absorption spectra that vary slowly across the visible with structures at the scale

[3] Author to whom correspondence should be addressed.

  

of 20 nm or more. However, the shapes of the spectra are often specific to the dyes and spectral imaging exploits this characteristic (Zhou *et al* 1996, Ornberg *et al* 1999).

Using trans-illumination, spectrally resolved information may be obtained by filtering the illumination source, for example, by using variable filters and acquiring a number of images. This approach, however, is somewhat inflexible for other types of microscopy. For example, when using fluorescence imaging, the imaging device must be capable of operating in a spectrally resolved manner. Additionally, the excitation source can benefit from being spectrally resolved (e.g. microspectrofluorimetry Kohen *et al* (1990)) though much useful information can be gained by using a single excitation wavelength band, in effect not optimally exciting all the fluorophores of interest. The characteristic fluorescence emission spectrum of each flurophore can be used to identify it and locate it spatially. This technique can be used to characterize cells *in vitro* or indeed with much larger biological samples.

Multiple band-pass filters placed immediately in front of the camera may be used to create a spectrally resolved imager. Although such a system may be simple to use and cost-effective for screening a specific set of dyes it is inflexible when compared to a tunable device that allows multiple screening procedures, inexpensively, with a single unit.

Several methods for achieving tunable spectral imaging microscopy have been put forward in recent years. The most promising of these involve the use of either a liquid crystal or acousto-optic spectral filter, or the use of a Sagnac interferometer. In summary, the use of an acousto-optic filter has advantages of speed (wavelength selection times of the order of microseconds), variable resolution (down to 1 nm) and a wide wavelength range (500–1000 nm). However, this is often a specialized and expensive solution. A liquid crystal filter is more cost-effective but this technique suffers from low transmission (<30%), limiting its application in fluorescence microscopy where signal intensities are low. A different approach, based on a Sagnac interferometer (Lavi *et al* 1998, Barshack *et al* 1999) is similarly specialized and expensive, offering a <10 nm resolution and <50% transmission. It has the additional disadvantage that a full spectral scan must always be captured precluding the possibility of faster partial scans or different dwell times at specific regions of the spectrum. This is particularly problematic when the signal is photon-limited, where the signal-to-noise ratio can be improved by optimizing the collection time. For a fuller review of techniques see Farkas (2001). All the above techniques require significant capital investment.

For this study, a system based around a linearly variable filter (LVF) was used incorporating novel hardware and software to produce a cost-effective solution of reasonable performance compared to other techniques. The additional cost of implementation on a conventional CCD camera-based microscopy system is less than £ 5000.

## 2. Experimental details

The spectral imaging device used for this study was developed and constructed in our Institute. It uses a standard monochrome CCD camera (type 4912, Cohu Inc., USA) though other types of imagers, with increased sensitivity or resolution may be used. The technique is quite capable of utilizing mega-pixel array imagers; we used a modest resolution imager to investigate the usefulness of the spectral imaging approach. The spectrally selective element is placed between the camera and the microscope output port using standard C-mount couplers and is based on a linearly variable dielectric band-pass filter together with novel drive hardware and acquisition software. The element has a resolution of 15 nm and covers the 400–700 nm band with a transmission of >40%. The system provides wavelength agility and allows for user-set dwell times. For this study, the spectrally resolved device was used with an upright microscope (Optiphot, Nikon, UK) equipped with a conventional fluorescence attachment. A range of achromatic objective lenses was used: 1.6× (0.05 NA), 10× (0.25 NA) and 20× (0.7 NA).

### *2.1. Image capture*

Images were captured into a personal computer (PC) using a 1 GHz processor (Dell, UK, Precision 220, 256 MB RAM) via a frame grabber (type PCI-1409, National Instruments Ltd., UK) and all software was written in the 'C' programming language under the LabWindows/CVI™ development environment (National Instruments Ltd., UK) and Windows 2000 operating system (Microsoft Corp., USA).

The system is capable of capturing the spectral image of an emissive sample in ∼10 s, spanning 400–700 nm in 6 nm steps (50 images). This capture arrangement was used in all examples shown unless otherwise stated. OD spectra were obtained by first capturing the spectral profile of the illumination through a blank part of the sample but of equivalent optical thickness and a 'black' image with no illumination. These images were used to correct the spectral image taken through the sample and to calculate the wavelength-dependant OD (OD(λ)) according to the equation:

$$\mathrm{OD}(\lambda) = -10 \log \left( \frac{I(\lambda) - I_{\mathrm{black}}}{I_{\mathrm{blank}}(\lambda) - I_{\mathrm{black}}} \right) \qquad (1)$$

where λ represents wavelength and $I$ the intensity at a single image pixel.

The data in the three-dimensional 'spectral image' could be presented in two ways: the complete spectrum at a particular pixel or as a series of images at selected narrow wavelength bands. The analysis of spectra at single pixels was usually the more interesting as this was used to identify the dominant dye present at that location. Furthermore, if two or more dyes were present at a pixel location, all contribute to the observed spectra. Primed with previously determined characteristic spectra of the dyes, the observations may be resolved through the application of linear un-mixing to determine the relative staining intensities. The supposition that individual component spectra combine linearly holds for both emissive samples and those characterized in terms of OD (or absorption coefficient) according to the Lambert–Beer absorption law.

The most appropriate additive combination of reference spectra that reproduce the observed spectrum can be determined by least squares fitting, as previously described (Farkas *et al* 1998). In this study we chose to use a non-negative

least squares algorithm (Lawson and Hanson 1974) since this approach cannot give rise to negative contributions that clearly have no physical meaning. Distribution maps for each constituent can thus be obtained from this un-mixing process. When un-mixing OD spectra, the results represent proportions of the reference spectra, having units of OD normalized to the references. The results of linear un-mixing have been represented in two ways. This normalized OD is mapped to pixel intensity such that areas of heavy staining appear bright in the resulting image, or alternatively, the dye distribution has been digitally extracted from the image by recreating the relative optical transmitted intensities by applying equation (1), in reverse, to the separated OD map of the particular dye. In this OD rendition of particular dyes, areas of heavy staining appear in dark colours and areas of light staining appear white (Levenson and Hoyt 2000).

Approximately 2 min were required to linear un-mix a complete image (768 × 576 pixels) on the 1 GHz PC using the non-negative least squares algorithm. However, strict code optimization has not been performed and it is believed that some speed may be gained in this application by initially formatting the data in memory in a more appropriate manner. The ever increasing speed of computers, in addition to the fact that this type of processing can be easily multithreaded since the same calculation is performed many times, independently, make much shorter processing times possible.

### 2.2. Standardized test samples

The system was characterized using a neutral density filter with areas of increasing OD from 0.04 to 1.0 (type X32-700, Edmund Optics Ltd., UK). Each section of the filter was imaged with the 10× objective, and the OD measured by averaging over a 10 × 10 pixel area. OD values were measured relative to the lowest OD section of the filter. The results were compared to corresponding values obtained with a spectrophotometer (type 8452A, Hewlett Packard, UK).

The capabilities and accuracy of the spectral linear un-mixing process was tested using samples fabricated from known, coloured absorptive filter samples. Test slides were made from plastic absorptive filters (Rosco, London, UK) of approximately 50–100 $\mu$m thickness. Sets of three partially overlapping filters were mounted on a microscope slide using aqueous mounting medium (Faramount, Dako, UK). The extinction coefficients of these samples were similar to those associated with conventional histological preparations. This approach was convenient since corresponding reference absorption spectra could be determined from a standard spectrophotometric approach.

### 2.3. Histology test samples

Human tumour biopsies (rectum and bladder) were used to provide singly and multiply stained histology sections. Formalin fixed and paraffin embedded tumours were used to provide 4 $\mu$m thick tissue sections, stained for glucose transporter (GLUT-1) or thymidulate synthase (TS) with and without a haematoxylin (Hx) counter-stain. Sections were de-waxed in xylene and rehydrated through graded alcohols to water and placed on microscope slides. The slides were immersed in 10 mM citric acid, pH 6, and heated for 12 min using an 800 W microwave oven (2450 MHz, Panasonic NN-6453BBPQ). The slides were then left to stand for 20 min before being washed in water. An auto-staining machine (Dako, UK) containing the detection reagents (ChemMate, Dako, K5001) and anti-GLUT-1 antibody, diluted to 1/200 or an anti-TS antibody, diluted to 1/300 were used. The auto-staining program included 30 min incubations in primary, secondary and tertiary reagents with 5 min in diaminobenzidine (DAB) substrate. Where required, the slides were then washed in water and counterstained in Mayer's haematoxylin for 10 s, then dehydrated in graded alcohols, cleared in xylene and mounted in DPX (VWR International, UK).

Tissue sections were also multiply stained for carbonic anhydrase IX (CA9) and pimonidazole (PIMO) were co-localization was expected. 4 $\mu$m sections were de-waxed in xylene and rehydrated through graded alcohols to water and placed on microscope slides. Slides were rinsed in water and then in Tris Buffer Saline (TBS) before incubation for 30 min in anti-CA9 antibody (provided by Harris, Oxford) diluted to 1/50. The slides were washed in TBS prior to the addition of alkaline phosphatase (Envision, Dako) and left to incubate for 30 min at room temperature. The slides were then washed in TBS before application of Vector Red substrate (Vector labs) and left to develop for 10 min. The slides were washed in buffer and then in water before demonstration of pimonidazole (Hydroxyprobe-1, supplied by Raleigh, University of North Carolina School of Medicine, Chapel Hill, NC, USA) which had been incorporated into a human bladder tumour by intravenous injection of 0.5 g $m^{-2}$ of pimonidazole in 100 ml of normal saline by a 15 min intravenous infusion between 18 h prior to a planned cystoscopy.

The bioreductively bound adducts were unmasked 0.01% pronase in PBS, pH 7.8, for 10 min. After washing well in water, endogenous peroxidase was blocked using peroxidase-blocking solution (Envision, Dako) for 5 min. Anti-pimonidazole IGg1 antibody (Natural Pharmacia International Inc., USA) diluted to 1/100 was then applied for 30 min. The slides were washed in buffer before the addition of horseradish peroxidase (Envision, Dako) and mouse polymer (Dako) for 30 min. After washing in buffer, DAB substrate was added (Envision, Dako) for 5 min. The sections were then washed in water, counterstained for 10 s in Mayer's haematoxylin before being dehydrated through graded alcohols, cleared in xylene and mounted in DPX (VWR International, UK).

## 3. Results

### 3.1. Absolute OD

It was important to characterize the OD performance of the spectral imaging microscope and camera, using the stepped neutral-density filter, since the accessible OD range ultimately determines the ability to decompose the spectral information and to provide quantitative information.

Figure 1 shows a comparison, at three wavelengths, of the OD measured on a spectrophotometer with the OD determined by the imager, over the range up to 1.0. The filter was imaged with the 10× objective and a 10 × 10 pixel area was averaged, with care taken to avoid any visible scratches. The graph

shows good agreement at low ODs, but noticeable variations for OD > 0.4. Near 1.0, variations of approximately 6% are present. This may be explained by differences in physical measurement areas of the two methods, but are considered reasonable bearing in mind that the maximum dynamic range of the imaging device is 256 : 1. Cumulative errors associated with CCIR video capture with frame grabbing boards (black level correction, DC restoration, etc) are such that it is unlikely that optical densities >1 could be determined accurately.

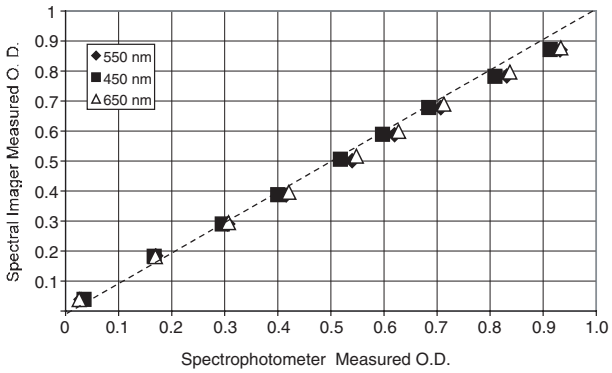


**Figure 1.** The OD of a stepped neutral density filter measured with the spectral imager and a diode array spectrophotometer at three wavelengths. The dotted line is a guide for the eye, with a slope of 1.0.

### *3.2. Spectral decomposition of test samples*

The results of un-mixing combinations of known coloured filters can be seen in figures 2 and 3. Figure 2 shows an image of three differently coloured filters obtained with the low power objective (1.6×) together with images showing the results of linear un-mixing represented as relative optical densities. The dark banding structure in the images was due to bubbles that formed as the mounting medium dried around the relatively thick filters. The reference spectra shown were obtained from the image data set, by averaging 100 × 100 pixel areas of the image where only single filters are present. They show that the three filters can be readily separated. This is however to be expected since the sample spectra are rather distinct. Nevertheless, it is instructive to compare the spectral imager performance with that obtained from a conventional RGB colour camera, with the three components undergoing a similar spectral un-mixing process. Images were taken on a conventional colour camera and new, 3-point reference spectra were acquired. The results of un-mixing are shown in figures 2(*g*)–(*i*) and indicate that although the filter separation with this limited data are quite accurate it has resulted in false positive responses. See, for example, figure 2(*i*) where there is some bleed through of the Pink filter (3) into the region of the Pale Blue filter (1).

Figure 3 shows the results of linear un-mixing of a much more challenging sample mixture, at the limit of the system's

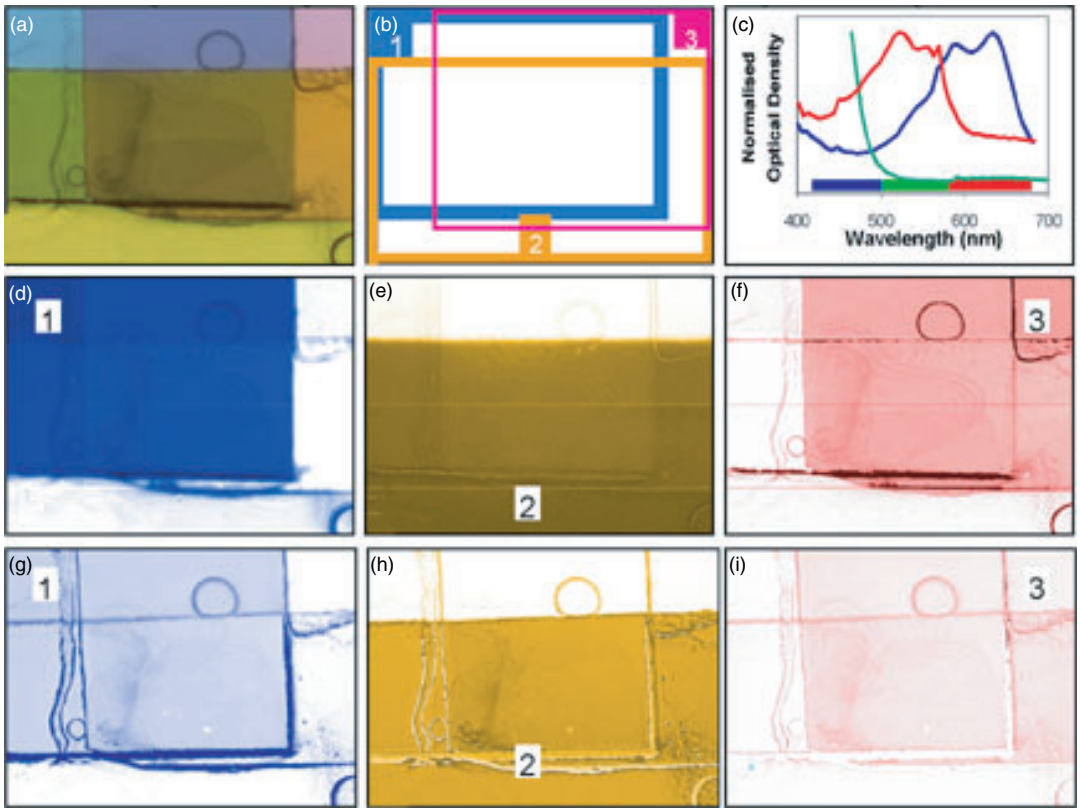


**Figure 2.** Spectral un-mixing of three overlapping differently coloured filters shown in (*a*) (filter extents are shown schematically in (*b*)). The reference spectra, as measured by the spectral imager, are shown in (*c*) for (1) pale blue (blue), (2) straw (green) and (3) no colour pink (red). The filters were digitally separated and are shown in (*d*)–(*f*). For comparison, a colour RGB image was un-mixed with reference spectra from the RGB image and the results are shown in (*g*)–(*i*). The approximate red/green/blue regions for a colour camera are shown on the *x*-axis of (*c*) for comparison.

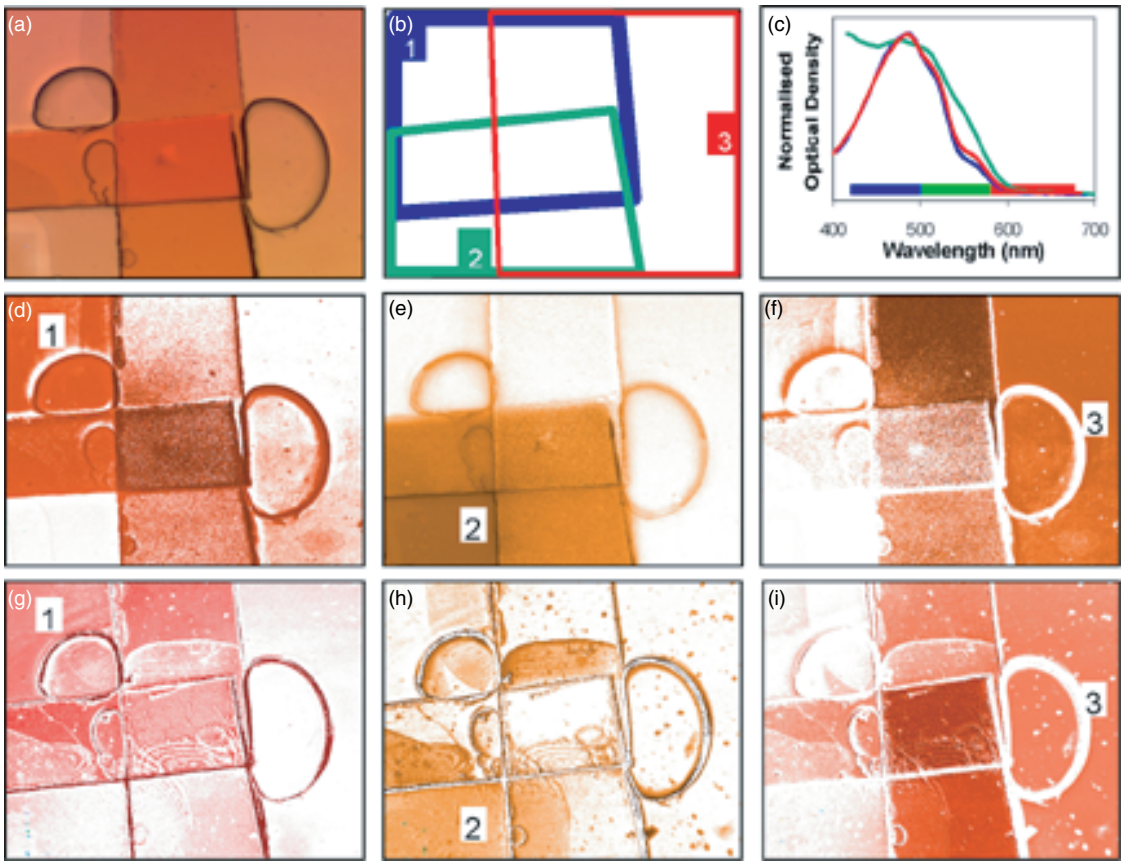


**Figure 3.** Spectral un-mixing of three overlapping filters of similar colour, shown in a (filter extents are shown schematically in (*b*)). The reference spectra, as measured by the spectral imager, are shown in (*c*) for (1) light flame (red), (2) apricot (green) and (3) flame (blue). The filters were digitally separated and are shown in (*d*)–(*f*). For comparison, a colour RGB image was un-mixed with reference spectra from the RGB image and the results are shown in (*g*)–(*i*). The approximate red/green/blue regions for a colour camera are shown on the *x*-axis of (*c*) for comparison.

performance. The three orange filters have very similar spectra and the results, as expected, are not as good as for the previous example. The reference spectra were obtained in the same way and are also shown. It is clear that maximum differences of only 0.05 OD units, in a very narrow wavelength range are present between two of the samples; the third sample, where the differences are present below 470 nm and are greater, is well separated. The result of un-mixing a RGB camera image is shown in figures 3(*g*)–(*i*) and the advantage of using the spectral imager is clear.

### *3.3. Spectral decomposition of histology samples*

Most clinical tumours contain a significant sub-population of hypoxic tumour cells (Hockel and Vaupel 2001, Vaupel *et al* 2001) which can be visualized immuno-histochemically through the intrinsic markers glucose transporter 1 (GLUT1) (Airley *et al* 2001) and carbonic anhydrase IX (CA9) (Wykoff *et al* 2000) and extrinsic hypoxic markers such as pimonidazole (PIMO) (Arteel *et al* 1998). An example of separating dyes from a multiply stained histological section is shown in figure 4. A section from a biopsy of bladder carcinoma was stained with PIMO (brown), CA9 (red) and Hx (blue). PIMO and CA9 are known markers of hypoxia and are expected to show considerable overlap in their localization in tumour tissue. Figures 4(*b*)–(*d*) show the results of digitally extracting these dye distributions from the image taken with the spectral imager and the 10× objective. In this case the reference spectra were taken from separate singly stained sections of the same biopsy (figure 4(*e*)). Representative, intensely stained areas of these sections were chosen by eye and a 5 × 5 pixel area was averaged. The results of un-mixing an image captured on a conventional RGB colour camera are also shown in figures 4(*f*)–(*h*). Most noticeable is the failure to detect much of the PIMO staining and the 'holes' left in the map of Hx staining due to heavily stained areas of PIMO and CA9.

It has been shown that markers, such as GLUT-1, can result in different spectral responses depending on their environment (Levenson and Farkas 1997, Barshack *et al* 1999). An example of separating such differences using spectral imaging is shown in figure 5. GLUT-1 bound to the cell membrane has a different brown hue to that present in the cytoplasm. Figure 5 shows intensity-mapped OD for the two species of GLUT-1 together with Hx in the separate RGB channels of the recreated image. This section of rectal carcinoma biopsy section was imaged with the 20× objective.

The spectral imager has also been used for the quantitative analysis of staining intensity. Tissue sections from rectal carcinoma biopsy were stained with TS and Hx. TS was strongly expressed in tumour areas. Figure 6(*a*) shows a colour

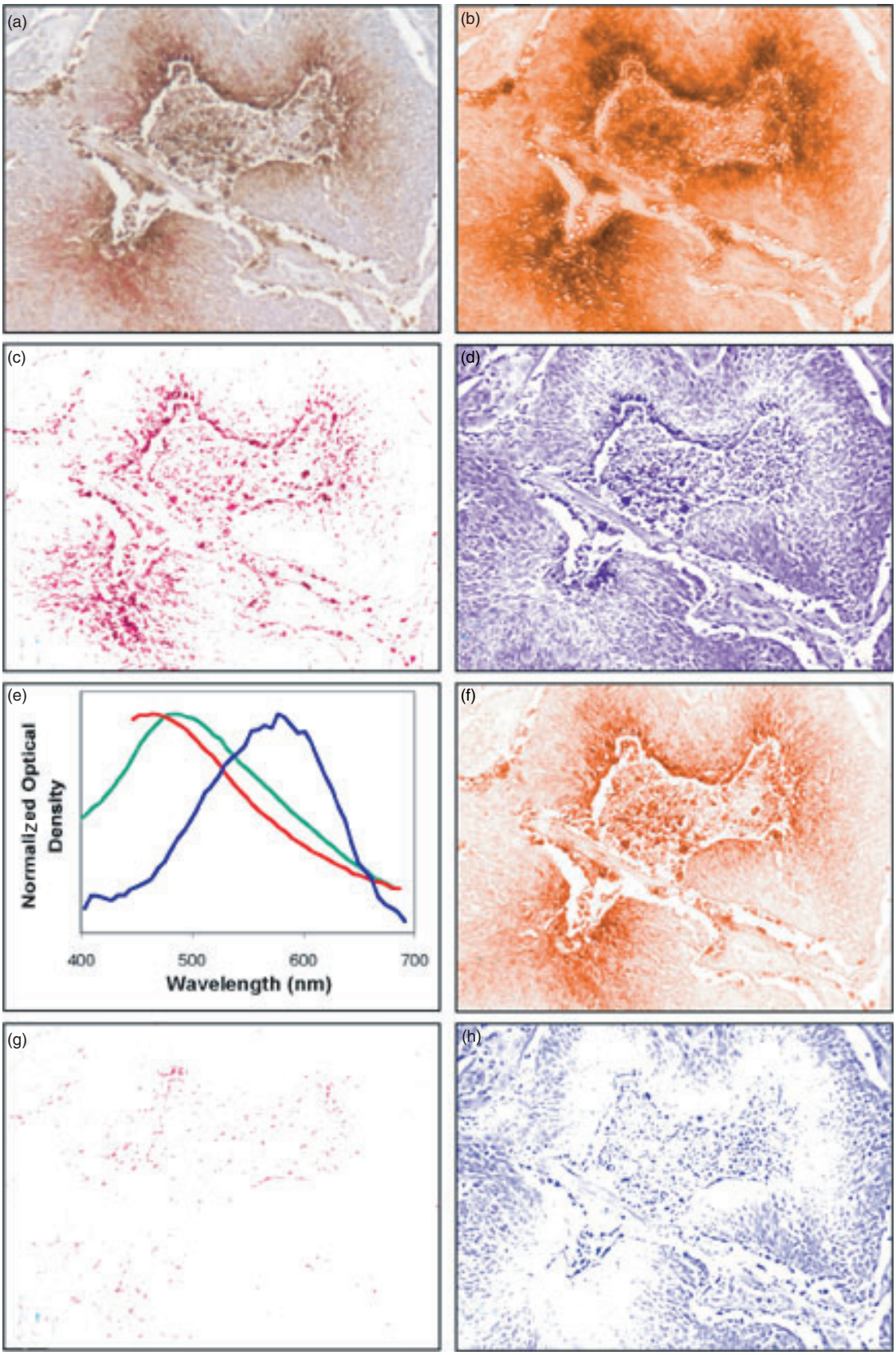


**Figure 4.** The tissue section (*a*) was stained with CA9 (red), PIMO (brown) and Hx (blue). These components have been spectrally unmixed and digitally separated into images (*b*)–(*d*), respectively using the reference spectra in (*e*). Images (*f*)–(*h*) show the results of un-mixing an RGB image.

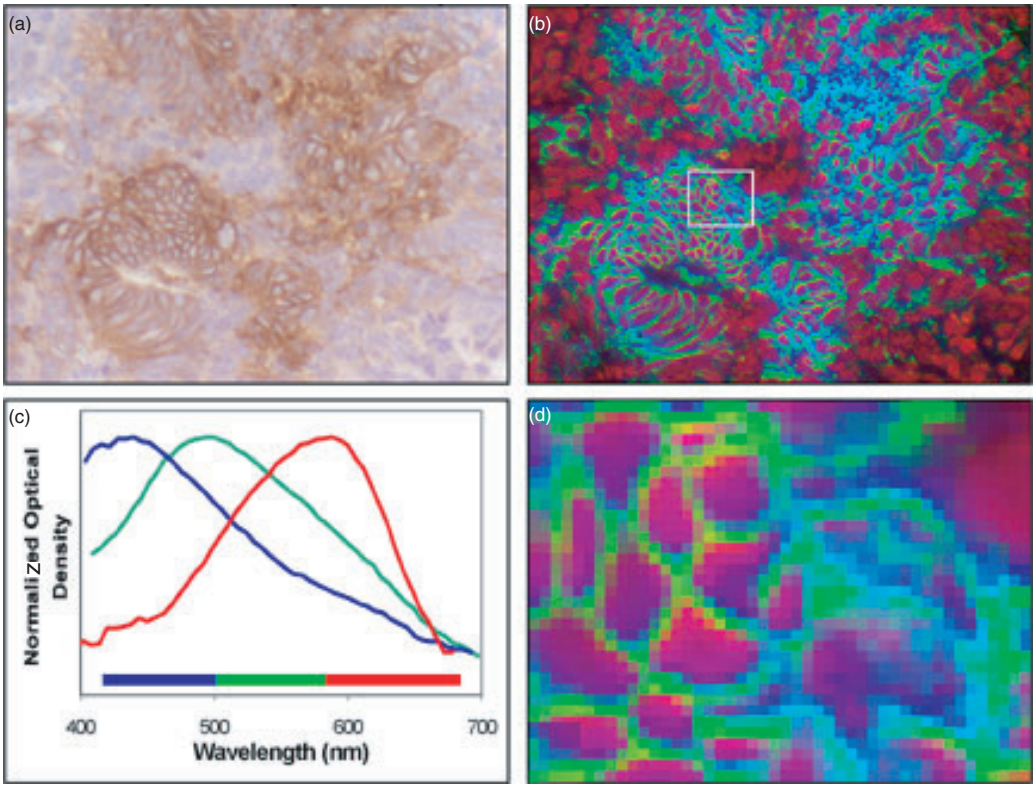


**Figure 5.** A tissue section stained with GLUT-1 and Hx (*a*) has been spectrally un-mixed to reveal the OD map of each component ((*b*) and zoomed region (*d*)). Cell-membrane-bound GLUT-1 (Green) has been separated from that in the cytoplasm (blue) and Hx (red). The spectra of these three components are shown in (*c*) with the same colour coding.

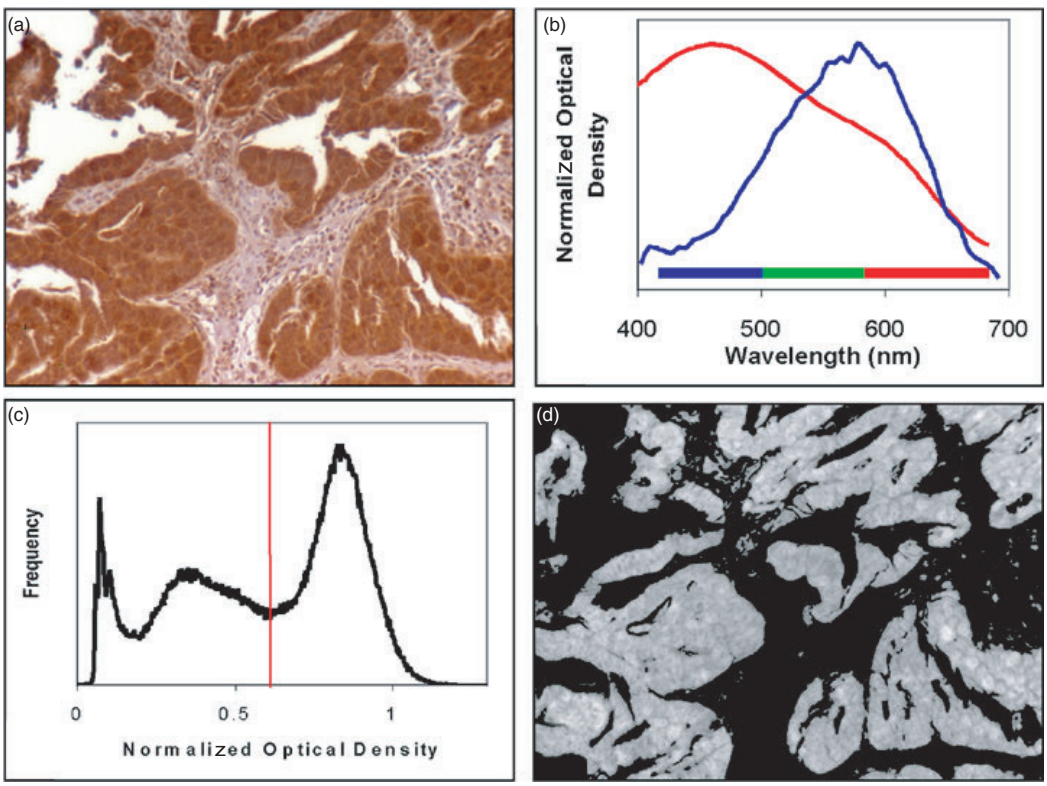


**Figure 6.** Quantitative analysis has been performed on tissue sections stained with TS (brown) and Hx (blue) (*a*). This was achieved by spectral un-mixing with reference spectra from singly stained samples (*b*) and plotting the histogram of TS staining density normalized to the reference spectra (*c*). Thresholding at 0.6 (red line in (*c*)) segments the areas of intense staining (light areas in image (*d*)) that are used to calculate an average staining density for the image.

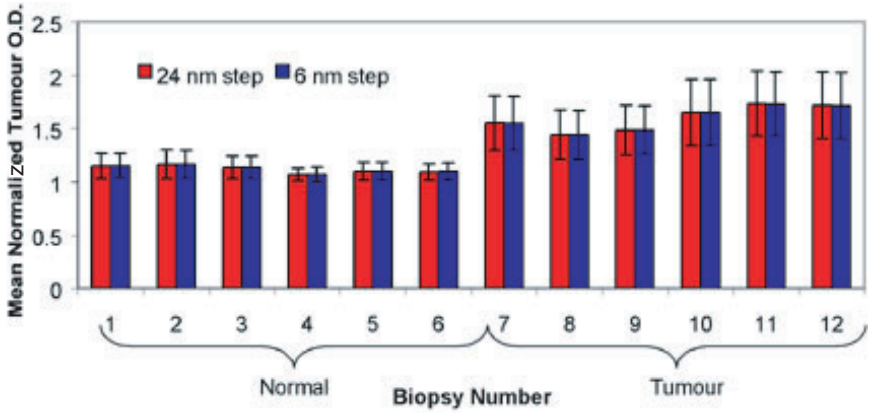


**Figure 7.** Reducing the amount of data by increasing the wavelength step size has a very small effect on the quantitative results of average TS stain intensity. The graph shows average staining intensity of the segmented region with error bars that represent the standard deviation of the pixel values.

image, through the 10× objective, of a heavily stained area. The spectral image was unmixed using the reference spectra shown, obtained from singly stained sections, to produce the map of TS staining in units of OD normalized to the reference spectrum. The histogram of TS staining is also shown in the figure and was used to segment the areas of strong staining for quantification. In this case a threshold of 0.6 provided good segmentation. In larger studies this threshold was fixed to a single value that was used for all sections. The areas of strong staining were then used to determine an average for the image. Using the average of all the pixels in the image as a quantitative measure would be highly dependant on the area of tissue chosen and the degree of tumour and stoma within it. Segmenting the strongly stained areas on the basis of stain intensity ensures that only the areas of interest contribute to the measure.

One advantage of this type of spectral imager is the ability to capture a data set with a reduced number of spectral points with the aim of increasing the speed of the acquisition and processing. Using a test sample of triply stained tissue, representative processing times to un-mix the full image were measured on the 1 GHz PC for different amounts of spectral information. All images were captured over the 400–700 nm spectral band but in varying steps. Increasing the step size from 6 to 12, 24, 48 and 96 nm decreased the processing time from 131 s to 95 s, 80 s, 71 s and 71 s, respectively (acquisition times reduced from 9.9 to 6.7, 4.5, 3.6 and 3.2 s). The results of quantitative analysis, similar to that for TS staining, were obtained to check the consistency of the results and it was found that step sizes of 6, 12 and 24 nm were within 15% of each other. Results for step sizes of 48 and 96 nm could differ significantly. The step size of 24 nm was chosen as an appropriate value for further imaging for this reason.

Spectral images of 12 tissue sections stained with TS and Hx were captured with a spectral step of 24 nm. The results of the quantitative analysis were compared with the result obtained with a 6 nm step, and the results are shown in figure 7. Single images from each biopsy were selected by eye and captured with the 10× objective. The error bars in the figure show the standard deviation of pixel values that contributed to the mean. As expected, the graph shows a significant difference between the normal and tumour tissue types.

### *3.4. Spectral analysis of fluorescence emission images*

As a further example and demonstration of spectral imaging applied to fluorescence microscopy the imager was used to provide qualitative screening of samples believed to undergo fluorescence resonance energy transfer (FRET) (Herman *et al* 2001). Breast carcinoma cells (MDA-MB-231) were tagged with green fluorescent protein (GFP), Cy3 and Cy5 *in vitro*. Under the spectral imaging microscope the GFP was excited with the integral UV lamp at around 480 nm. Where the fluorescent molecules are sufficiently close to each other (<10 nm) FRET is thought to occur, transferring energy in a cascade from the GFP to the Cy3 to the Cy5. Figure 8 shows three images from samples containing GFP alone, GFP and Cy3, and GFP, Cy3 and Cy5 together with representative spectra from bright areas of the images. The results of linear un-mixing have been shown by superimposing reference spectra onto the graphs to demonstrate how they contribute to the full spectral shape.

## 4. Discussion

Several examples of the application of a novel and cost-effective spectral imager to microscopy in biology have been presented. In addition, the imager and processing software has been tested on a known sample of varying OD and on samples of known absorptive filter combinations.

### *4.1. Spectral decomposition of test samples*

The test of OD measurement accuracy showed some differences between the measurements made on a spectrophotometer and those made with the spectral imager. These differences are believed to be due to local variations in OD, due to scratches, that affect the microscopic measurement of the imager to a greater extent than the overall measurement of the spectrophotometer and due to the means of capturing the image information. We would expect these differences to be much reduced through the use of a higher dynamic range digital camera.

The results of un-mixing combinations of filters of known spectral characteristics demonstrate the ability of the imager,

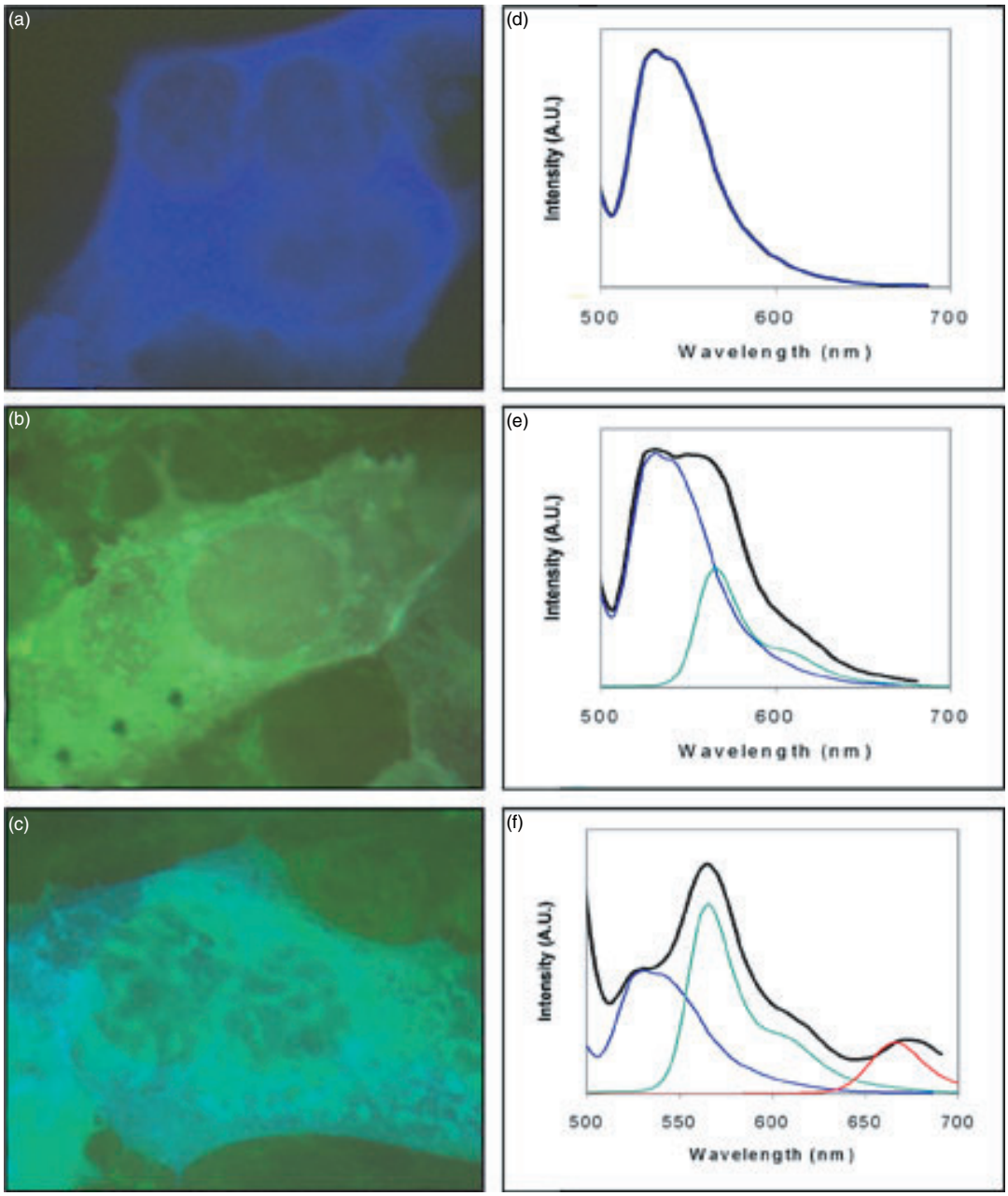


**Figure 8.** The analysis of fluorescence from samples of breast carcinoma cells, *in vitro*, containing GFP (*a*), GFP and Cy3 (*b*), GFP, Cy3 and Cy5 (*c*). Images (*a*)–(*c*) show the spectrally un-mixed components mapped to the blue (GFP), green (Cy3) and red (Cy5) channels on the image. Graphs (*d*)–(*f*) show representative spectra from a bright part of the image (black) with the GFP (blue), Cy3 (green) and Cy5 (red) reference spectra superimposed in their un-mixed proportions.

with a resolution of 15 nm, to separate very similar spectra. The system was able to separate the visually similar 'flame' filter from the 'light flame' filter throughout most of the test image, on the basis of spectral shape alone. Results were optimum where single filters were imaged in distinct regions of the image but the separation of these two filters where the overlap was also successful.

### *4.2. Spectral decomposition of histology samples*

It has been shown that this system, in combination with non-negative linear un-mixing, is able to separate dye distributions from multiply stained histological tissue. We have successfully segmented the brown stain of diaminobenzidine and the red stain of Vector Red from the light blue of haematoxylin. However, the process is extendable to any combination of dyes with spectral profiles that are sufficiently different. The results of un-mixing known filter combinations (figure 3) suggest that these differences may be extremely subtle. It has also been shown that the different patterns of diaminobenzidine staining colour can also be separated (figure 5), when tagged to membrane-bound GLUT-1 compared to GLUT-1 contained within the cytoplasm.

Quantitative studies have also been undertaken to measure the degree of TS expression in normal and tumour tissue

sections. These show that the spectral imager can separate and measure the OD of TS staining and show a significant difference between tumour and normal tissue. Furthermore, it has been shown that in this type of study the data set can be reduced by a factor of 4 by increasing the wavelength step size without significantly affecting the results. This has benefits in decreased acquisition and processing time.

### *4.3. Spectral analysis of fluorescence emission images*

We have also demonstrated the use of the system in fluorescence microscopy for the detection of FRET by the un-mixing of the fluorophores GFP, Cy3 and Cy5. This qualitative indication of FRET using the spectral imaging microscope allows rapid screening of samples prior to more quantitative exploration with fluorescence lifetime imaging (Ng *et al* 1999).

In fluorescence microscopy, quantitative image analysis is often performed and the addition of a spectrally resolved device enhances this capability to a significant extent. A common problem is associated with filter bleed-through, or where the characteristics of the emission filter are perhaps not always best suited to the fluorophore of interest. The availability of the complete emission spectrum is extremely helpful when determining fluorophore co-localization or performing studies involving bleaching (e.g. fluorescence recovery after photobleaching).

### *4.4. Conclusions*

Comparisons with conventional colour camera imaging of histological samples show clear advantages in the ability to segment features of interest, since the absorption spectra of the chromophores are both broad and unlikely to match the colour camera's filter bands. Moreover, the use of spectral imaging opens up the possibility of performing quantitative measurements, at least in terms of chromophore concentrations relative to known standards. Here, it must be stressed that care must be exercised in the preparation and staining protocols to ensure consistency.

In conclusion, the principle current disadvantage is the processing time; however, code optimization, improvements in processor speed and the ability to use multiple processors will enhance the range of applications. It should be pointed out that the chromatic performance of the optical instrument should also be optimized. While modern plan apochromatic objectives are very good indeed, the chromatic performance of the illumination should not be neglected, especially with low dynamic range imagers such as the one used in this study. To a large extent, a 'flat' spectral response is inherently obtained by normalizing the image acquisition process, but this will be successful only as long as a sufficiently large signal is provided by the imager at all wavelengths. It is thus important to ensure that the illumination spectral variations and illumination stability are adequate. In practice, we have found that the use of tungsten lamps, in conjunction with a stable power supply and colour temperature correction filters is satisfactory.

We have demonstrated that the use of an instrument with moderate bandwidth performance can contribute significantly to the range of microscopy applications in biology. The cost-effectiveness of our approach is considered particularly advantageous since the device is easily added to existing camera-based microscopy installations. Although most of the data presented here utilizes the full spectral range, the wavelength agility of the device allows operation over a restricted range, optimized for the specific application. A corresponding reduction of computation time can thus be achieved.

## Acknowledgments

The authors gratefully acknowledge the help of S Chandarama in data collection and S Ameer-Beg, T Ng, N Edme and M Keppler for the loan of the FRET samples. It is a pleasure to acknowledge the technical support of R Newman, J Prentice and R Locke for electronic, mechanical workshop and interface coding assistance respectively. We should also like to thank A Harris and J Raleigh for the provision of histological markers and antibodies and the referees for their comments. This work was funded by Cancer Research UK, programme grant C133/A1812–SP2195-01/02.

## References

Airley R, Loncaster J, Davidson S, Bromley M, Roberts S, Patterson A, Hunter R, Stratford I and West C 2001 *Clin. Cancer Res.: An Official J. Am. Assoc. Cancer Res.* **7** 928–34

Arteel G E, Thurman R G and Raleigh J A 1998 *Eur. J. Biochem.* **253** 743–50

Barshack I, Kopolovic J, Malik Z and Rothmann C 1999 *Br. J. Cancer* **79** 1613–19

Farkas D L 2001 *Methods in Cellular Imaging* ed A Periasamy (Oxford: Oxford University Press) pp 345–61

Farkas D L, Du C, Fisher W, Lau C, Niu W, Wachman E S and Levenson R M 1998 *Comput. Med. Imag. Graphics* **22** 89–102

Herman B, Gordon G, Mahajan N and Centonze V 2001 *Methods in Cellular Imaging* ed A Periasamy (Oxford: Oxford University Press) pp 257–72

Hockel M and Vaupel P 2001 *Sem. Oncol.* **28** 36–41

Kohen E, Kohen C, Prince J, Schachtschabel D O, Hirschberg J G, Morliere P, Santus R, Dubertret L and Shapiro B L 1990 *J. Biotechnol.* **13** 1–27

Lavi M, Milman U, Cabib D, Garini Y, Gil A, Juta T and Adel M 1998 *Proc. SPIE* vol 3261, pp 313–21

Lawson C L and Hanson R J 1974 Solving Least Squares Problems (New Jersey: Prentice-Hall) 1995 revised edition (SIAM Society for Industrial and Applied Mathematics)

Levenson R M and Farkas D L 1997 *SPIE Proc.* vol 2983, pp 123–35

Levenson R M and Hoyt C C 2000 *Am. Lab.* 26–33

Ng T *et al* 1999 *Science* **283** 2805–9

Ornberg R L, Woerner B M and Edwards D A 1999 *J. Histochem. Cytochem.* **47** 1307–13

Vaupel P, Kelleher D K and Hockel M 2001 *Sem. Oncol.* **28** 29–35

Wykoff C C *et al* 2000 *Cancer Res.* **60** 7075–83

Zhou R, Hammond E H and Parker D L 1996 *Medical Phys.* **23** 1977–86